Strengthening Mechanisms and Hall-Petch Stress of ultrafine grained Al-0.3%Cu

Huang, Tianlin; Shuai, Linfei; Wakeel, Aneela; Wu, Guilin; Hansen, Niels; Huang, Xiaoxu

Published in:
Acta Materialia

Link to article, DOI:
10.1016/j.actamat.2018.07.006

Publication date:
2018

Document Version
Peer reviewed version

Accepted Manuscript

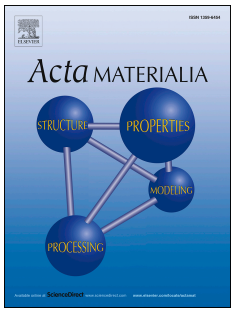

Strengthening Mechanisms and Hall-Petch Stress of ultrafine grained Al-0.3%Cu

Tianlin Huang, Linfei Shuai, Aneela Wakeel, Guilin Wu, Niels Hansen, Xiaoxu Huang

PII: S1359-6454(18)30530-5

DOI: 10.1016/j.actamat.2018.07.006

Reference: AM 14683

To appear in: *Acta Materialia*

Received Date: 20 March 2018

Revised Date: 22 June 2018

Accepted Date: 2 July 2018

Please cite this article as: T. Huang, L. Shuai, A. Wakeel, G. Wu, N. Hansen, X. Huang, Strengthening Mechanisms and Hall-Petch Stress of ultrafine grained Al-0.3%Cu, *Acta Materialia* (2018), doi: 10.1016/j.actamat.2018.07.006.

Strengthening Mechanisms and Hall-Petch Stress of ultrafine grained Al-0.3%Cu

Tianlin Huang[a,b,*], Linfei Shuai[a] , Aneela Wakeel[a] , Guilin Wu[a,**], Niels Hansen[a,c] , Xiaoxu Huang[a,d]

[a] *Joint International Laboratory for Light Alloys (MOE), College of Materials Science and Engineering, Chongqing University, Chongqing 400045, China*

[b] *Electron Microscopy Center of Chongqing University, Chongqing University, Chongqing 400045, China*

[c] *Technical University of Denmark, Risø Campus, DK-4000 Roskilde, Denmark*

[d] *Department of Mechanical Engineering, Technical University of Denmark, DK-2800 Kgs. Lyngby, Denmark*

*Corresponding author: huangtl@cqu.edu.cn (Tianlin Huang)

**Corresponding author: wugl@cqu.edu.cn (Guilin Wu)

Abstract

An ultrafine grained Al-0.3wt. %Cu has been produced by cold rolling to a thickness reduction of 98% (ε_{vM}=4.5). The deformed structure is a typical lamellar structure with a boundary spacing of 200nm as characterized by transmission electron microscopy (TEM) and electron backscatter diffraction (EBSD). Coarsening of the deformed structure to recrystallization is achieved by heat treatment in the range of 100~300℃. Good thermal stability has been observed up to 175℃ with some segregation of Cu to the boundaries as observed by 3D atom probe characterization. Tensile tests have shown a flow stress (0.2% offset) of 198MPa with continuous flow with no yield drop and Lüders elongation. To quantify the contribution of boundary strengthening to the flow stress, dislocation strengthening and solid solution hardening have been calculated and subtracted from the flow stress. It has been found that boundary strengthening can be expressed by a Hall-Petch relationship and that these constants in this equation are in very good agreement with precious observation of recrystallized pure polycrystalline aluminium with a grain size in the tens of micrometer range. Thereby the Hall-Petch relationship of aluminium can be extended an order of magnitude from the micrometer to the sub-micrometer range, which is of both scientific and technical importance.

Keywords: Ultrafine grained, Thermal stability, Strengthening, Ductility, Hall-Petch slope

1. Introduction

The flow stress of polycrystalline metals and alloys increases with decreasing grain size as formulated in the Hall-Petch relationship [1-4]:

$$\sigma(\varepsilon) = \sigma_0(\varepsilon) + k(\varepsilon)d^{-0.5} \quad (1)$$

where d is the grain size and $\sigma_0(\varepsilon)$ and $k(\varepsilon)$ are constants independent of the grain size. Eq. (1) has guided extensive research and development to increase the strength of metallic materials by reducing the grain size, with an increase in strength following the structural refinement as predicted by Eq. (1) [4-8]. However, when the grain size is reduced to the micrometer/sub-micrometer scale, it has been found that $k(\varepsilon)$ is no longer independent of the grain size. Examples are Al [9-12] and IF steel [9, 13, 14] deformed by accumulative roll bonding (ARB) and spark plasma sintered Al [15, 16] and Cu [17, 18]. The effect of a reduction in grain size in the micrometer/sub-micrometer scale has been related to strengthening mechanisms other than boundary strengthening that can raise $k(\varepsilon)$. Such mechanisms can be a reduced density of mobile dislocations or an increase in the dislocation source strength. We suggest also that the flow of material during a tensile test may have to be considered. This is because samples showing a deviation from Eq. (1) show discontinuous flow during tensile testing, giving rise to yield drop and Lüders elongation. In the present study we have therefore examined the grain size strengthening in a material with an ultrafine grain size which shows continuous flow in tension. This material is pure aluminum (99.9996%) alloyed with 0.3%Cu, where it has been found that the stress-strain curves are continuous over the grain size range from 0.2 to 50 μm [19],

stabilized by the Cu content in the structure. Samples with different small grain sizes can therefore be produced allowing a validation of Eq. (1). Such a validation requires that the strength contribution from boundaries σ_{GB} can be estimated independently of other contributions to the strength such as dislocation strengthening , solid solution strengthening and particle hardening. An important part of the study is therefore a quantification of the different strength contributions based on quantification of strengthening parameters by transmission electron microscopy (TEM), electron backscatter diffraction (EBSD) and three-dimensional atom probe (3DAP) investigations. As to the purity of aluminum, we have chosen super pure aluminum (99.9996%) to remove effects caused by the presence of impurities. The samples are tested in tension, also including a determination of the uniform elongation before necking.

Based on the quantification of microstructure, texture, chemistry and mechanical behavior, the following will be addressed: (i) the effect of adding 0.3%Cu in solid solution on the structural and mechanical stability of super-pure Al, (ii) strengthening mechanisms and their contributions to the macroscopic flow stress of deformed and annealed samples, and (iii) Hall-Petch strengthening related to the presence of deformation induced boundaries compared with boundary strengthening in polycrystalline Al [3]. The mechanical behavior has been analyzed by tensile testing at room temperatures at a strain rate which allows a direct comparison with a previous study [3] of Hall-Petch strengthening in polycrystalline pure aluminium.

2. Materials and experimental procedure

The original material used in this study is an Al-0.3%Cu alloy ingot, which was produced by combining ultra-high purity (99.9996%) Al with 0.3 wt.% OFHC Cu. The ingot was hot-isostatic pressed at 200 ºC into a thick plate, from which a slab of dimensions of $300 \times 300 \times 50$ mm^3 was cut and then cold-rolled to a thickness reduction of 98% (corresponding to ε_{vM}=4.5). After each rolling pass, the sample was quenched into liquid-nitrogen-cooled alcohol to limit the influence of heat generation during rolling. The cold rolled sample was annealed for 1 h at temperatures between 100 and 300 ºC to obtain samples with different boundary spacings/grain sizes. The deformed and annealed microstructures were characterized by TEM and EBSD. Foils for TEM investigation were prepared by twin jet electropolishing [20] and were examined using a JEOL JEM2100 electron microscope operated at 200 kV. An online Kikuchi-line analysis system [21] installed in the microscope with a misorientation resolution of 0.1º was used for crystallographic orientation measurements. Samples for SEM investigation were polished in a 1:9 (volume fraction) $HClO_4$:C_2H_5COOH solution at −20 ºC and 20 V for 45 ~ 60 seconds and studied using a FEI Nova400 FEG-SEM equipped with a Channel5 EBSD system. All the TEM and SEM observations were made in the longitudinal section (containing the normal direction, ND and rolling direction, RD).

The microstructure and misorientations of the as-deformed and low-temperature-annealed samples were also investigated using transmission Kikuchi diffraction (TKD) using an Oxford Instruments AZtec system equipped on a JOEL

7800F FEG-SEM, to take advantage of the higher spatial resolution of this technique. The distribution of elemental Cu was characterized by 3DAP analysis. The 3DAP samples were prepared by electropolishing and characterized using a CAMECA LEAP4000HR equipment.

Tensile specimens (gauge dimensions of 26.25 mm long, 12.25 mm wide and 1.00 mm thick) were machined from the as-deformed and annealed samples. Tensile tests were carried out using a SHIMAZU AG-X10 electronic universal testing machine at an initial strain rate of 2×10^{-4} /s at room temperature. The tensile elongation was measured using an extensometer of gauge length 25 mm.

3. Results

3.1. Microstructure and microstructural evolution

3.1.1. Deformation microstructure and parameters

Fig. 1 shows the microstructures in the deformed state as seen in a TEM. A fine lamellar structure is observed with extended boundaries parallel to the rolling plane. Between these boundaries that interconnecting dislocation boundaries can be observed. The two types of boundaries have been dubbed geometrically necessary boundaries (GNBs) and incidental dislocation boundaries (IDBs) [22]. The GNB spacing (D^{GNB}) was measured using an intercept method along the direction perpendicular to the GNBs from TEM images, with a resulting average spacing of about 200 nm, which is similar but slightly lower than values reported for commercial purity AA1100 and AA1050

deformed by 6 cycles ARB processing (ε_{vM}=4.5) [9, 10, 12, 23]. The boundary spacing between the IDBs (D^{IDB}) was measured along the direction parallel to the GNBs, giving an average IDB boundary spacing of 780 nm. Boundary misorientations across both the GNBs and IDBs were measured using the online Kikuchi-line analysis system in the TEM. An example set of data is given in Fig. 1, showing both a TEM micrograph of an investigated area (Fig. 1a) and a sketch illustrating the boundary misorientation in the same area (Fig. 1b). In the sketch, thin red lines, thin solid lines and thick solid red lines indicate boundaries with misorientation angles $\theta < 3°$, $3° \leq \theta \leq 15°$ and $15° < \theta$, respectively. The long straight lamellar boundaries (GNBs) are predominantly high angle boundaries, and most of the interconnecting boundaries (IDBs) are dislocation boundaries with misorientations below 15°. The distributions of misorientation angle across GNBs and IDBs are shown in Figs. 1c and 1d. The data demonstrate that the GNBs are medium to high angle boundaries, whereas IDBs mostly are boundaries with misorientation angles lower than 5°. The average misorientation of IDBs is determined as 3.6°. Both IDBs and GNBs appear as very narrow boundaries when viewed edge on. No accumulation of dislocations at GNBs is observed.

Between the GNBs and IDBs, isolated dislocations were also observed. The dislocation density varies from crystallite to crystallite. Typically, dislocations only in one row of lamellar grains were clearly observed at a selected two-beam condition, due to the fact that there is a large difference in orientation across the lamellar boundaries, but only small orientation difference between the interconnecting boundaries in a given lamella. The dislocation density was estimated therefore from the dislocation spacing

measured from 20 ~ 30 images, with the sample thickness measured using a convergent beam electron diffraction (CBED) method. The density of these isolated dislocations was determined to be 1.75×10^{14} m^{-2}, which is referred to as ρ_0 in the calculation of strength from dislocation contribution (see Section 4).

To clarify the distribution of elemental Cu, 3DAP characterization was performed. The images in Fig. 2 show the distribution of Cu in a volume with a dimension of $65\times69\times475$ nm^3. In Fig. 2a, blue dots show Al atoms and red dots show Cu atoms. Fig. 2b shows more clearly that the Cu element is distributed non-uniformly. In particular, a very high concentration of Cu segregation is observed in a linear feature, which is interpreted as a grain boundary segregation. The presence of a grain boundary was confirmed by analysis of crystallographic poles obtained from the two sides of the boundary. Near the boundary, a low concentration area of Cu can also be seen from Fig. 2b, but only on one side. At the other side of the boundary, the concentration of Cu is similar to that of the matrix. To illustrate the Cu distribution, a line analysis along the sample (indicated by the black dashed line in Fig. 2b) was made. The result (Fig. 2c) shows that the Cu concentration at the grain boundary is close to 3.6 wt.%, which is about 12 times the nominal concentration (0.3 wt.%). Similar observations of Cu segregation at a grain boundary have also been reported in a nanostructured Al-2.5%Cu alloy [24].

3.1.2. Microstructural evolution during annealing

To investigate the thermal stability of the ultrafine grained Al-0.3%Cu and to obtain samples with different grain sizes, the as-deformed samples were annealed at

temperatures between 100 and 300 ºC for one hour and the structural evolution was examined. Fig. 3 illustrates by EBSD maps the structure of the samples after annealing at 100, 175, 200 and 225 ºC. It was found that, after annealing at 100 ºC (Fig. 3a), the major change is structural coarsening without a significant change in the lamellar morphology. It can be clearly seen that the lamellar boundaries are not as straight as those in the deformed structure, and that the lamellar grains have become more equiaxed. As shown in Table 1, also the density of dislocations between boundaries, ρ_0 shows a decrease. Fig. 3b shows the microstructure after annealing at 175 ºC where some recrystallization grains can also be found in the recovered lamellar structure. The volume fraction of the recrystallized grains is about 14%, and their distribution in the structure is inhomogeneous. A cause may be the non-uniform deformation structure, where the stored energy depends on the crystallographic orientation of the individual grains [25, 26]. After annealing at 200 ºC (Fig. 3c), the microstructure is still partially recrystallized, and consists of large recrystallized grains (typically a few μm in size) in a recovered microstructure. The volume fraction of the recrystallized grains is $\sim$ 90%. The recovered areas have a subgrain size near to 1 μm, and the sub-grains are equiaxed. After annealing at 225 ºC and higher temperatures, the samples are fully recrystallized. The recrystallized grain structure observed in the sample annealed at 225 ºC is shown in Fig. 3d.

From the above analysis, the microstructural evolution during annealing can be classified into three stages, namely recovery at temperatures below 150 ºC, nucleation and partial recrystallization in the range of 175 - 200 ºC, and full recrystallization at

temperatures higher than 225 ºC.

Values of D^{GNB} and D^{IDB} were measured for the samples annealed up to 175 ºC. At least 500 measurements were obtained for each sample. The variation of average values as a function of annealing temperature is shown in Fig. 4. The differences between D^{GNB} and D^{IDB} are relatively large in the as-deformed and recovered states, as the lamellar grains have an elongated shape along the RD. It can be seen that both D^{GNB} and D^{IDB} increase only slowly with increasing temperature. Note that the D^{GNB} values are all less than 1 μm at this stage. Based on the values of D^{GNB} and D^{IDB}, an equivalent boundary spacings (D_E) can be calculated and treated as grain size of the lamellar structure. The method for calculation of D_E is given in section 4.1. For the fully recrystallized conditions, the grain sizes were measured by an intercept method with randomly oriented lines on EBSD maps. After partial recrystallization when annealing at 175 - 200 ºC, the samples have a bimodal microstructure. Therefore the sizes of the recrystallized grains and the recovered sub-grains were accordingly measured separately. Then, the D_E of the partially recrystallized structure can be calculated based on the value of the D_E of the non-recrystallized area, grain size of the recrystallized grains and their volume fraction. The measured and calculated grain size/D_E are listed in table. 1.

The misorientation angles across boundaries of the samples annealed at temperatures up to 175 ºC were measured by TEM Kikuchi diffraction. Among the IDBs, there are a large number of low angle boundaries. The fraction of low angle boundaries (< 3º) in

the GNBs and IDBs, and their average misorientations are shown in Table 1. Note in this table that the structural coarsening is reflected in the increasing value of D^{GNB} and in the slow decrease in the fraction of IDBs with $\theta < 3°$. It follows that both GNBs and IDBs contribute significantly to the flow stress in the recovery region.

The dislocation density between the GNBs and IDBs (ρ_0) of the 100 - 175 ºC annealed samples was also measured by TEM. For every sample, 3 ~ 5 measurements were made at different areas. The average values of dislocation density and their standard deviations are shown in Table 1. It can be seen that the dislocation density decreases slowly with increasing annealing temperature. An illustration of the structural stability in this material is a high dislocation density $\simeq 1.2 \times 10^{14}\, m^{-2}$ after annealing at 150 ºC. This means that ρ_0 also contributes significantly to the strength of recovered samples.

3.1.3. Texture

Texture was characterized by EBSD for all the samples. After cold rolling, a typical rolling texture of Al composed of Brass ({110} (112)), Copper ({112} (111)) and S ({123} (634)) [27] was observed. The near-center layer is dominated by Brass texture components (~ 60%), and the surface regions have comparable volume fractions of Copper, S and Brass, see also Refs. 25 and 26. After low temperature annealing the texture does not change significantly, but when the annealing temperature is increased to above 225 ºC, a strong Goss ({011} (100)) texture has been developed in the center regions.

Taylor factors (assuming tensile deformation along RD) for the as-deformed and 150 ºC -annealed samples were both calculated to be 3.05. For the partially recrystallized sample (annealed at 175 ºC), the Taylor factor was calculated as 3.18. The influence of the Taylor factor on the flow stress is considered in Section 4.2.

3.1.4. Particles

From the TEM images (Fig. 1a), it can be seen that there are very few second phase particles present in the Al matrix. The average distance of the particles is larger than a few micrometers, and it follows that most of Cu is present in solid solution. The particle density has not been measured precisely due to the small number. Nevertheless, after annealing at temperatures higher than 200 ºC, a large number of particles have precipitated in the matrix and at the grain boundaries [28]. The particle density of the 250 ºC annealed sample was measured from SEM electron channeling contrast (ECC) images and the average spacing between the particles was determined to be ~ 1.9 µm.

3.2. Mechanical properties

The stress-strain curves of the as deformed and annealed samples are summarized in Fig. 5. The as-deformed sample has a flow stress (0.2% offset) of 198 MPa, a UTS of 224 MPa and a total elongation of ~ 5%. The strength is close to that seen in nanostructured AA1050 and AA1100 with 0.5 ~ 1.0 percent of impurities produced by accumulative roll bonding (ARB) [9, 29]. The elongation is slightly lower than the reported value for these alloys (~ 7%). However, the gauge length of the tensile specimen (26 mm) used in the present study is much larger than that used for the

tensile testing of AA1050 and AA1100 in the previous studies (10 mm). As an increase in gauge length may affect the total elongation negatively [30], it is concluded that the tensile ductility of the present ultrafine grained Al-0.3%Cu alloy is comparable to that of the previously studied nanostructured AA1050 and AA1100 samples.

For the samples annealed with increasing temperature in the low temperature range, the strength gradually decreases, but a yield drop and Lüders elongation, as seen in AA1050 or AA1100 [9, 29], are not observed. This is discussed in Section 5.

After annealing at medium temperatures (175 - 200 ºC), where partial recrystallization of the samples takes place, the flow stress decreases, and the tensile elongation (both uniform and total elongation) increases. Similar to the recovered samples, the tensile stress-strain curves show a continuous work hardening behavior. After annealing at 190 ºC for one hour, the total elongation reaches more than 15% with the flow stress maintaining a value of about 100 MPa, illustrating the significant effect of the Cu present in the matrix. For the fully recrystallized samples (annealing at temperatures higher than 225 ºC), the mechanical behavior is very similar to that of other coarse grained pure and commercial pure Al materials. The flow stress decreases very slowly with increasing grain size and the elongation barely changes.

In Table 2 the summary of mechanical properties shows that the flow stress $\sigma_{0.2}$ of Al-0.3%Cu can be increased 7 ~ 8 times by cold rolling. And, only 25% of this strength is lost by annealing at 150 ºC, illustrating the stability of the alloy by the extended window for recovery.

4. Analysis

4.1 Structural parameters

The parameters to be considered include the grain size/boundary spacing, the boundary misorientations, the dislocation density, and the Cu concentration in the matrix.

The dislocation density between the boundaries ρ_0 is measured directly, and is given in Table 1. However, a large part of the total dislocation content is stored in the low angle dislocation boundaries. A former study [11] shows that the critical misorientation angle between grain boundary strengthening / Hall-Petch strengthening and dislocation strengthening / Taylor strengthening in Al can be estimated to be 2 ~ 3º. In this study, we chose 3º as the critical misorientation, and accordingly boundaries with misorientations below and above 3º are treated separately. The fraction of boundaries with misorientation below 3º in the IDBs is defined as $f_{<3^\circ}^{IDB}$ and their average misorientation as $\theta_{<3^\circ,av}^{IDB}$. In the GNBs, the boundaries with misorientation below 3º are relatively few and classified as $f_{<3^\circ}^{GNB}$ with an average misorientation $\theta_{<3^\circ,av}^{GNB}$.

The surface area of the GNBs and IDBs, can be expressed as follows [31]:

$$S_V^{GNB} = \frac{1}{D^{GNB}} \tag{2}$$

$$S_V^{IDB} = \frac{\pi}{2D^{IDB}} \tag{3}$$

Then, the total surface area per unit volume with misorientation lower than 3º, can be expressed:

$$S_V^{<3^\circ} = \frac{f_{<3^\circ}^{GNB}}{D^{GNB}} + \frac{\pi f_{<3^\circ}^{IDB}}{2D^{IDB}} \quad (4)$$

And, the surface area of the boundaries above 3º is:

$$S_V^{GB} = S_V - S_V^{<3^\circ} = \frac{1-f_{<3^\circ}^{GNB}}{D^{GNB}} + \frac{\pi\left(1-f_{<3^\circ}^{IDB}\right)}{2D^{IDB}} \quad (5)$$

The dislocation density (ρ_{LB}) stored in the boundaries with misorientation angles below a critical angle (θ_c) can be calculated as follows:

$$\rho_{LB} = \int_0^{\theta_c} S_\theta \rho_A \, d\theta \quad (6)$$

where S_θ is the surface area of boundaries with a misorientation of θ, and ρ_A is the dislocation density per unit area of boundary, which is proportional to the misorientation angle across the dislocation boundary. For a mixed tilt and twist boundary, ρ_A can be expressed as [32]:

$$\rho_A = 1.5\,\theta/b \quad (7)$$

where θ is misorientation angle across the boundary and b is Burgers vector (0.286 nm for Al). From Eq. (5), (6) and (7), the density of the dislocations which are stored in the low angle boundaries ρ_{LB} can be written as:

$$\rho_{LB} = \frac{1.5 f_{<3^\circ}^{GNB} \theta_{<3^\circ,av}^{GNB}}{D^{GNB} b} + \frac{1.5\pi f_{<3^\circ}^{IDB} \theta_{<3^\circ,av}^{IDB}}{2D^{IDB} b} \quad (8)$$

For the as deformed and recovered structure, an equivalent boundary spacing can be calculated from the density of GNBs and IDBs, in which the low angle (< 3º) dislocation boundaries should be omitted. For an equiaxed grain structure, the total surface area per volume can be expressed as $S_V = 2/D_R$, where D_R is the grain size.

An equivalent boundary spacing (D_E) of the lamellar structure can therefore be calculated by the relationship:

$$D_E = \frac{2}{S_V^{GB}} \quad (9)$$

For the partially recrystallized samples, the surface areas of the recovered and recrystallized volumes are calculated separately. Since the recrystallized grains are almost equiaxed, the total surface area of the partially recrystallized samples can be written as:

$$S_V = S_V^{GB}(1 - V_{Rex}) + \frac{2}{D_{Rex}} V_{Rex} \quad (10)$$

Where D_{Rex} is the average size of the recrystallized grains.

The values of ρ_{LB} for the partially recrystallized samples can be calculated in the same way as described above by application of Eq. (8), though it should be noted that for this we only use data for the non-recrystallized (i.e. recovered) volumes.

The calculated values of D_E and ρ_{LB} are listed in Table 1. The error bars given are based on the accuracy of the misorientation measurements by Kikuchi diffraction (0.1º).

The average Cu concentration in the matrix (C_0) has been obtained by 3DAP. In this study, boundary segregation of Cu has also been observed, which will lower the average value of C_0 in the matrix. The values of C_0 for the as-deformed, 100, 150, and 200 ºC annealed sample obtained from the 3DAP data are 0.20, 0.18, 0.13 and 0.11 wt.%, respectively.

4.2. Strength calculation

The Hall-Petch relationship shows large variations both in $k(\varepsilon)$ and $\sigma_0(\varepsilon)$. when the grain sizes are refined to the sub-micrometer level. Such variations may be caused by additional strengthening mechanisms besides boundary strengthening, to be taken into account. In Al-0.3%Cu such mechanisms are dislocation strengthening and solid solution strengthening. Additionally, in the fully recrystallized samples, there is also a strength contribution from dispersed particles (negligible in the as-deformed and recovered samples). The flow stress of Al-0.3%Cu can therefore be expressed [4, 33]:

$$\sigma_s = \sigma_0 + \sigma_{GB} + \sigma_{dis} + \sigma_{ss} + \sigma_p \quad (11)$$

where σ_0, σ_{GB}, σ_{dis}, σ_{ss} and σ_p are contributions from the lattice friction, grain boundaries, dislocations, elements in solid solution and particles, respectively. All contributions resist dislocation glide and we apply simple superposition based on a quantification of these contributions. To apply simple superposition as a mean to underpin the development of strong metals for engineering applications has been discussed (see for example ref. [34]). It can also be noted that superposition in line with Eq. 1 has been addressed [35] by separating boundary strengthening from contribution from other sources in aluminum.

For the 99.999%Al, the friction stress $\sigma_0 = 5.5\,MPa$ was determined experimentally for pure aluminum [3]. In the as-deformed sample, $\sigma_p \simeq 0$ and in the fully recrystallized samples $\sigma_{dis} \simeq 0$.

Strengthening due to Cu in solid solution can be expressed as [36]:

$$\sigma_{ss} = 2AC_0^{2/3} \quad (12)$$

where A is a constant (=12.4 for Cu in the Al matrix [36]) and C_0 is the concentration of the solute in weight percent.

The strength from dislocation contribution can be expressed as proportional to the square root of the total dislocation density (Taylor strengthening) [37]:

$$\sigma_{dis} = M\alpha Gb\sqrt{\rho_0 + \rho_{LB}} \quad (13)$$

In this equation, M is the Taylor factor. G is the shear modulus (=26 GPa for Al). ρ_0 is the dislocation density between the dislocation boundaries and ρ_{LB} is the density of dislocations stored in low angle boundaries, when IDBs are present in a large density. α is a constant (0.24) which has been obtained for coarse grained aluminum tested in tension [38] to different strains. α decreases with increasing strain and 0.24 is an average. The decrease in α relates to an increase in the dislocation density causing a decrease in $\ln(R/b)$, where R is the cutoff distance [37], which decreases as the dislocation density is raised. In Table 1 the dislocation density $(\rho_0 + \rho_{LB})$ is high of the order as in the tensile deformed aluminum [38], thus $\alpha = 0.24$ is considered to be a good estimate of this empirical parameter.

After annealing at 200 ~ 250 ℃, precipitation has been observed. The contribution from particle strengthening can be calculated by [39-41]:

$$\sigma_p = B\frac{Gb}{2\pi}\frac{1}{D_{Af}}\ln(D_{Af}/b) \quad (14)$$

where B is a constant equal to 1 for edge dislocations and to $1/(1-v)$ (where v is Poisson's ratio) for screw dislocations, and D_{Af} is the average particle spacing on the surface, which can be measured from SEM-ECC images.

The calculated results of σ_{ss}, σ_{dis} and σ_p are plotted in Fig. 6. Note that for the partially recrystallized sample, the calculated value of σ_{dis} has been multiplied by a factor of $(1-V_{Rex})$. Based on the above, the strength contribution arising only from boundary strengthening can be calculated. For the as-deformed and recovered samples, $\sigma_{GB} = \sigma_{0.2} - \sigma_0 - \sigma_{ss} - \sigma_{dis}$, and for the fully recrystallized samples, $\sigma_{GB} = \sigma_{0.2} - \sigma_0 - \sigma_{ss} - \sigma_p$. The calculated σ_{GB} is also plotted in Fig. 6.

5. Discussion

The addition of 0.3% Cu to super-pure aluminum has increased the mechanical and thermal stability in a way that an ultrafine structured strong material can be produced by cold rolling to large strain. When deforming this material in tension the plastic flow is continuous without a yield drop and/or Lüders elongation. The material is therefore suitable for an analysis of both stabilizing and strengthening mechanisms, which will be addressed under the following themes: (i) stabilizing effect of Cu in solid solution, (ii) strengthening mechanisms (solid solution strengthening, dislocation strengthening and boundary strengthening) and (iii) Hall-Petch relationship.

5.1. Stabilizing effect of Cu in solid solution

In the processing of nanostructured material by plastic deformation to high strain, it is important to limit dynamic and static recovery mechanisms. Such an effect can be achieved through addition of alloying element or small particles. The efficiency of Cu is demonstrated by a summary of literature data given in Table 3, where the efficiency

can be demonstrated by a fine boundary spacing (d_t) and high density of dislocations (ρ_0) stored in the volume between deformation induced boundaries. This comparison shows that except for the Al-1%Si [42] and AA8011 [43], which contain a large number of nano-particles to stabilize the microstructure, the boundary spacings of the Al-0.3%Cu, AA1100, AA1050, 99.99%Al and Al-2.5%Cu [24] alloys, can all be related to Cu concentration. With higher Cu concentration, the grains can be refined to a smaller size by plastic deformation to a comparable strain. The stabilizing effect of Cu also remains during annealing: after 1h at 175 ºC, ρ_0 is still high ($0.65 \times 10^{14}\ m^{-2}$) whereas commercial purity (99.5%) Al, ρ_0 at the end of recovery is one or two orders of magnitude smaller [12].

The stabilizing effect of adding solute atoms to a pure metal may have its cause in segregation to, and pinning of, structural defects as dislocation, dislocation boundaries and high angle boundaries. Such segregation is observed by 3DAP and an example of segregation to a single grain boundary is given in Fig. 2. Additionally, a large number of boundaries have been characterized and it appears that there is a strong tendency for Cu to segregate at medium angle dislocation boundaries and high angle boundaries. It is also observed that the concentration of Cu between the boundaries decreases with increasing annealing temperature, although it is still significant both in deformed and recovered samples.

Besides its thermal stability, Al-0.3%Cu also exhibits a good mechanical stability. This is demonstrated through the tensile behavior shown in Fig. 5, where tensile elongation with increasing strain without the presence of a yield drop and/or Lüders

elongation is seen. This is in strong contrast to the mechanical behavior of commercial purity aluminum deformed to high strain and subsequently annealed. The tensile behavior of such samples have no elongation in the deformed state and show a yield drop and Lüders elongation after annealing [9, 29]. Note that all the samples in Fig. 5 show strain hardening with a uniform elongation that increases with annealing temperature to 2 ~ 3%. The observed mechanical stability of Al-0.3%Cu may have its cause in the stability of the dislocation structure that evolves in the volume between the lamellar boundaries. The large density of dislocations ($\rho_0 + \rho_{LB}$) can supply dislocation sources and mobile dislocations, thereby stabilizing the mechanical behavior. It is therefore achieved by plastic deformation to large strain to produce a high strength light material which is both mechanically and thermally stable combined with good ductility.

5.2. Strengthening mechanism

5.2.1. Solid solution strengthening

Solid solution strengthening comes from the resistance of the solute atoms to dislocation glide, and is controlled by the concentration (C_0) of solute atoms in the matrix. Assuming all the Cu atoms (0.3%) are in solid solution, the strength contribution calculated from the solid solution strengthening is 11.2 MPa. However, due to the segregation of Cu atoms to the grain boundaries, as shown in Fig. 2, the actual concentration of Cu in the solid solution is lower than 0.3%. As a consequence, the solid solution strengthening is expected to be less than 11.2 MPa. Based on the estimated Cu content in the solid solution for the as-deformed sample and the annealed

samples, the solid solution strengthening was calculated, showing a variation of 5.4 ~ 8.9 MPa (Fig. 6).

5.2.2. Dislocation strengthening

Table 3 shows that the contribution of σ_{dis} for the deformed and recovered structure is significant. The reason for this is the high density of dislocations between the boundaries, which is typical for ultrafine grained metals such as AA1050 [12], AA1100 [9] and interstitial free steel [5, 9] produced by deformation to large plastic strains. Nevertheless, the dislocation density in these ultrafine grained metals decreases very fast during annealing, which causes a very fast decrease of the flow stress. In the present Al-0.3%Cu alloy, the dislocation density still remains at a high level after annealing. This lower rate of dislocation annihilation causes a slower decrease of the yield strength compared to other plastically deformed metals, and therefore a larger window of recovery. Thus, the effect of Cu is marginal on solid solution strengthening, but it is significant on dislocation strengthening through pinning of a high density of dislocations in the volume between the lamellar boundaries.

5.2.3. Boundary strengthening

The contribution of the boundary strengthening to the flow stress depends on the spacing between boundaries and their resistance to dislocation glide. The spacing is calculated based on the assumption of a critical angle (~ 3º) above which the boundaries are assumed to be impenetrable to dislocations (see Eq. 9). As to the boundary resistance to dislocation glide, it may be affected by the extensive

segregation of Cu to the boundaries. However, the boundary resistance in Al is relatively small due to the high stacking fault energy [44]. This means that pile up stresses can easily be relaxed by cross-slip of dislocations near boundaries into the parent grain or in the neighboring grain. We may, therefore not expect a significant effect of segregation on the boundary resistance to dislocation glide. In this context it is noteworthy that precise measurement of the Hall-Petch slope in pure (99.99%) and impure (99.5%) aluminum shows a lower Hall-Petch slope in the latter [3], where some boundary segregation of elements such as Fe and Si must be expected.

5.3. Hall-Petch relationship

The Hall-Petch relationship as expressed in Eq. (1) was proposed in 1962 [45] to relate the flow stress at a given strain to the reciprocal square root of the grain size. This formulation together with an equation relating the yield stress and fracture stress to the grain size [1,2] has since been debated and many alternative relationships have been proposed. Examples are a replacement of the grain size with the dislocation density in the deformed grains [46, 47] where good correlations have been obtained. A discussion of such alternative formulations is however outside the scope of the present study where parameters and methodology have been chosen to validate the contribution of grain boundaries strengthening to the flow stress of a polycrystalline material as expressed in Eq (1). However, when using this equation to different systems large variations have been observed in both $\sigma_0(\varepsilon)$ and $k(\varepsilon)$. Examples are aluminum and interstitial free steel deformed to large strain and subsequently recovered, where $\sigma_0(\varepsilon)$ and $k(\varepsilon)$ may change significantly when the boundary spacing is reduced to the

sub-micrometer level [9-11, 48, 49]. Variations in $\sigma_0(\varepsilon)$ and $k(\varepsilon)$ may have their cause in strengthening mechanisms that contribute to the flow stress in addition to boundary strengthening. In the present study we have assumed that such mechanisms are lattice strengthening, solid solution strengthening, dislocation strengthening and particle strengthening. Eq. (1) can therefore be rewritten as follows [50]:

$$\sigma(\varepsilon) - \sigma_0 - \sigma_{ss} - \sigma_{dis} - \sigma_p = kd^{-1/2} \quad (15)$$

Based on the values in Table 3, the reduced flow stress is plotted in Fig. 7 against the reciprocal square root of the equivalent boundary spacing. This figure shows a slope of 45.0 $MPa\mu m^{1/2}$ and a flow stress of about zero at an infinite boundary spacing. This finding is in very good accordance with observations showing a slope of 40 $MPa\mu m^{1/2}$ in pure aluminum and 25 $MPa\mu m^{1/2}$ in 99.5% aluminium [3]. We have also calculated the slope for offset other than 0.2%, see Fig. 8. The good agreement observed in Fig. 7 and Fig. 8 between the strength contribution for boundaries and the reciprocal square root of the equivalent boundary spacing, and the agreement with previous observation in polycrystalline aluminum, support an extension of the Hall-Petch relationship from the micrometer to the sub-micrometer scale. This is a novel finding of both scientific and technological importance.

6. Conclusions

Al-0.3% Cu has been cold-rolled to a reduction of 98% ($\varepsilon_{vM} = 4.5$) to produce an ultrafine structure subdivided by dislocation boundaries and lamellar, medium to high

angle boundaries. Deformed samples have been annealed to recovery and recrystallization and tested in tension. The conclusions are the following:

1. The addition of 0.3% Cu to super-pure Al (99.9996%) stabilizes the deformation structure allowing the grain size to be reduced to the sub-micrometer scale. By atom probe analysis it has been found that there is a strong segregation of Cu to medium and large angle boundaries to a concentration 10 times larger than in the surrounding matrix.

2. Tensile straining of deformed and annealed samples shows good mechanical stability with no yield drop and Lüders elongation and both deformed and annealed sample show strain hardening with a uniform elongation increasing with annealing temperature to 2~3%.

3. The combination of mechanical and structural stability has allowed a quantification of structural parameters and a calculation of solid solution strengthening and dislocation strengthening. Thereby it has been possible to calculate the contribution from boundary strengthening in the submicrometer polycrystalline structure.

4. The contribution of boundary strengthening is proportional to the reciprocal square root of the equivalent boundary spacing. The observed slope is in accordance with the Hall-Petch relationship established in polycrystalline aluminum, thereby widening the application of the Hall-Petch equation (Eq. 1) scaling the flow stress to the grain size one order of magnitude from the micrometer to the sub-micrometer scale.

Acknowledgments

The authors wish to thank the financial support of the Natural Science Foundation of China (NSFC, Grants No. 51327805, 51471039 and 51421001), State Key Research and Development Program of MOST of China (2016YFB0700401, 2016YFB0700403). NH thanks the support of the 111 Project (B16007) by the Ministry of Education and the State Administration of Foreign Experts Affairs of China. The authors thank Prof. A. Godfrey and Prof. D. Juul Jensen for helpful discussions and careful review of the manuscript.

References

[1] E. Hall, The deformation and ageing of mild steel: iii discussion of results, Proc. Phys. Soc. London, Sect. B 64 (1951) 747-753.

[2] N. Petch, The cleavage strength of polycrystals, J. Iron Steel Inst. 174 (1953) 25-28.

[3] N. Hansen, The effect of grain size and strain on the tensile flow stress of aluminium at room temperature, Acta Metall. 25 (1977) 863-869.

[4] N. Hansen, Hall-Petch relation and boundary strengthening, Scr. Mater. 51 (2004) 801-806.

[5] N. Tsuji, N. Kamikawa, R. Ueji, N. Takata, H. Koyama, D. Terada, Managing both strength and ductility in ultrafine grained steels, ISIJ Int. 48 (2008) 1114-1121.

[6] X. Liu, H. Zhang, K. Lu, Strain-induced ultrahard and ultrastable nanolaminated structure in nickel, Science 342 (2013) 337-340.

[7] R. Z. Valiev, Y. Zhu, Recent findings in superior strength and ductility of

ultrafine-grained materials, Trans. Mater. Res. Soc. Jpn 40 (2015) 309-318.

[8] M. Meyers, A. Mishra, D. Benson, Mechanical properties of nanocrystalline materials, Prog. Mater. Sci. 51 (2006) 427-556.

[9] N. Tsuji, Y. Ito, Y. Saito, Y. Minamino, Strength and ductility of ultrafine grained aluminum and iron produced by ARB and annealing, Scr. Mater. 47 (2002) 893-899.

[10] C. Yu, P. Kao, C. Chang, Transition of tensile deformation behaviors in ultrafine-grained aluminum, Acta Mater. 53 (2005) 4019-4028.

[11] N. Kamikawa, X. Huang, N. Tsuji, N. Hansen, Strengthening mechanisms in nanostructured high-purity aluminium deformed to high strain and annealed, Acta Mater. 57 (2009) 4198-4208.

[12] J. Kidmose, Structural optimization of nanostructured aluminum for enhancing mechanical properties and formability, PhD Thesis, Technical University of Denmark (2014).

[13] S. Gao, A. Shibata, M. Chen, N. Park, N. Tsuji, Correlation between continuous/discontinuous yielding and Hall-Petch slope in high purity iron, Mater. Trans. 55 (2014) 69-72.

[14] S. Gao, M. Chen, M. Joshi, A. Shibata, N. Tsuji, Yielding behavior and its effect on uniform elongation in IF steel with various grain sizes, J. Mater. Sci. 49 (2014) 6536-6542.

[15] G. Le, A. Godfrey, N. Hansen, W. Liu, G. Winther, X. Huang, Influence of grain size in the near-micrometre regime on the deformation microstructure in

aluminium, Acta Mater. 61 (2013) 7072-7086.

[16] G. Le, A. Godfrey, N. Hansen, Structure and strength of aluminum with sub-micrometer/micrometer grain size prepared by spark plasma sintering, Materials & Design 49 (2013) 360-367.

[17] K. Zhu, Q. Ruan, A. Godfrey, The kinetics of grain growth in near-micrometre grain size copper produced by spark plasma sintering, in: IOP Conference Series: Materials Science and Engineering, Vol. 89, IOP Publishing, 2015, p. 012060.

[18] K. Zhu, A. Godfrey, N. Hansen, X. Zhang, Microstructure and mechanical strength of near and sub-micrometre grain size copper prepared by spark plasma sintering, Materials & Design 117 (2017) 95-103.

[19] A. Wakeel, T. Huang, G. Wu, T. Yu, N. Hansen, X. Huang, Structure and mechanical properties of nanostructured Al-0.3%Cu alloy, in: 35th Risø International Symposium on Materials Science: New Frontiers of Nanometals, 2014, pp. 463-469.

[20] G. Christiansen, J. Bowen, J. Lindbo, Electrolytic preparation of metallic thin foils with large electron-transparent regions, Mater. Charact. 49 (2002) 331-335.

[21] Q. Liu, A simple and rapid method for determining orientations and misorientations of crystalline specimens in TEM, Ultramicroscopy 60 (1995) 81-89.

[22] D. A. Hughes, N. Hansen, The microstructural origin of work hardening stages, Acta Mater. 148 (2018) 374-383.

[23] Q. Liu, X. Huang, D. Lloyd, N. Hansen, Microstructure and strength of

commercial purity aluminium (AA1200) cold-rolled to large strains, Acta Mater. 50 (2002) 3789-3802.

[24] L. Jiang, J. Li, P. Cheng, G. Liu, R. Wang, B. Chen, J. Zhang, J. Sun, M. Yang, G. Yang, Microalloying ultrafine grained Al alloys with enhanced ductility, Sci. Rep. 4 (2014) 3605:1-6.

[25] X. Li, A. Wakeel, T. Huang, G. Wu, X. Huang, Recrystallization textures and microstructures of Al-0.3%Cu alloy after deformation to high strains, in: IOP Conference Series: Materials Science and Engineering, Vol. 89, IOP Publishing, 2015, p. 012032.

[26] A. Wakeel, T. Huang, G. Wu, O. V. Mishin, X. Huang, Development of a strong goss texture during annealing of a heavily rolled Al-0.3%Cu alloy, in: IOP Conference Series: Materials Science and Engineering, Vol. 82, IOP Publishing, 2015, p. 012050.

[27] A. Rollett, F. Humphreys, G. S. Rohrer, M. Hatherly, Recrystallization and related annealing phenomena, Elsevier, 2004.

[28] L. Shuai, T. Huang, G. Wu, N. Hansen, X. Huang, Characterization of Cu distribution in an Al-0.3%Cu alloy cold rolled to 98%, in: IOP Conference Series: Materials Science and Engineering, Vol. 219, IOP Publishing, 2017, p. 012038.

[29] I. Topic, H. W. Höppel, D. Staud, M. Merklein, M. Geiger, M. Göken, Formability of accumulative roll bonded aluminum AA1050 and AA6016 investigated using bulge tests, Adv. Eng. Mater. 10 (2008) 1101-1109.

[30] Y. Zhao, Y. Guo, Q. Wei, T. Topping, A. Dangelewicz, Y. Zhu, T. Langdon, E.

Lavernia, Influence of specimen dimensions and strain measurement methods on tensile stress-strain curves, Mater. Sci. Eng. A 525 (2009) 68-77.

[31] A. Godfrey, D. Hughes, Determination of boundary area and spacing in prismatic structures with applications to dislocation boundaries, Mater. Charact. 48 (2002) 89-99.

[32] D. Hughes, N. Hansen, Microstructure and strength of nickel at large strains, Acta Mater. 48 (2000) 2985-3004.

[33] X. Zhang, N. Hansen, A. Godfrey, X. Huang, Dislocation-based plasticity and strengthening mechanisms in sub-20 nm lamellar structures in pearlitic steel wire, Acta Mater. 114 (2016) 176-183.

[34] A. S. Argon, Strengthening mechanisms in crystal plasticity, Oxford University Press, Oxford (2008).

[35] J. T. Al-Haidary, N. J. Petch and E. De Los Riso, The plastic deformation of polycrystalline aluminium, in: T.N. Baker (Editor), Yield, flow and fracture of polycrysatls, Applied Science Publishers LTD, 1983, pp. 33-49.

[36] M. Dixit, R. Mishra, K. Sankaran, Structure-property correlations in Al 7050 and Al 7055 high-strength aluminum alloys, Mater. Sci. Eng. A 478 (1) (2008) 163-172.

[37] D. Kuhimann-Wilsdorf, Theory of plastic deformation: properties of low energy dislocation structures, Mater. Sci. Eng. A 113 (1989) 1-41.

[38] N. Hansen, X. Huang, Microstructure and flow stress of polycrystals and single crystals, Acta Mater. 46 (5) (1998) 1827-1836.

[39] N. Hansen, Dispersion strengthening of aluminium-aluminium-oxide products, Acta Metall. 18 (1) (1970) 137-145.

[40] E. Orowan, Symposium on Internal Stresses in Metals and Alloys, Oct. 15-16 (1947), p. 451. Institute of Metals (1948).

[41] A. J. Foreman, M. J. Makin, AERE-R 5201 (1966).

[42] T. Huang, Q. Dong, X. Gong, N. Hansen, Q. Liu, X. Huang, Cold rolled nanostructured super-pure Al (99.9996%) containing 1% Si particles: structure and strength, J. Mater. Sci. 47 (2012) 7914-7920.

[43] H.-W. Kim, S.-B. Kang, N. Tsuji, Y. Minamino, Elongation increase in ultrafine grained Al-Fe-Si alloy sheets, Acta Mater. 53 (2005) 1737-1749.

[44] R. W. Armstrong, Hall-Petch Relationship: Use in Characterizing Properties of Aluminum and Aluminum Alloys, in: G. E. Totten, M. Tiryakioglu, O. Kessler (Eds.), Encyclopedia of Aluminum and Its Alloys, CRC Press, 2017, pp. 1-30.

[45] R. W. Armstrong, I. Codd, R. M. Douthwaite, N. J. Petch, The plastic deformation of polycrystalline aggregates, Phil. Mag. 7 (1962) 45-58.

[46] J. C. M. Li, Petch relation and grain boundary sources, Trans. Metall. Soc. AIME 277 (1963) 239-47.

[47] H. Conrad, S. Feuerstein, L. Rice, Effects of grain size on the dislocation density and flow stress of niobium. Mater. Sci. Eng. 2 (1967) 157–168.

[48] H. W. Höppel, J. May, M. Göken, Enhanced strength and ductility in ultrafine-grained aluminium produced by accumulative roll bonding, Adv. Eng. Mater. 6 (9) (2004) 781-784.

[49] Y. Cao, L. He, Y. Zhou, P. Wang, J. Cui, Contributions to yield strength in an ultrafine grained 1050 aluminum alloy after DC current annealing, Mater. Sci. Eng. A 674 (2016) 193-202.

[50] N. Hansen, Flow stress and grain size dependence of non-ferrous metals and alloys, in: T.N. Baker (Editor), Proceedings of the Yield, Flow and Fracture of Polycrystals, Applied Science Publishers LTD, 1983, p. 311-350.

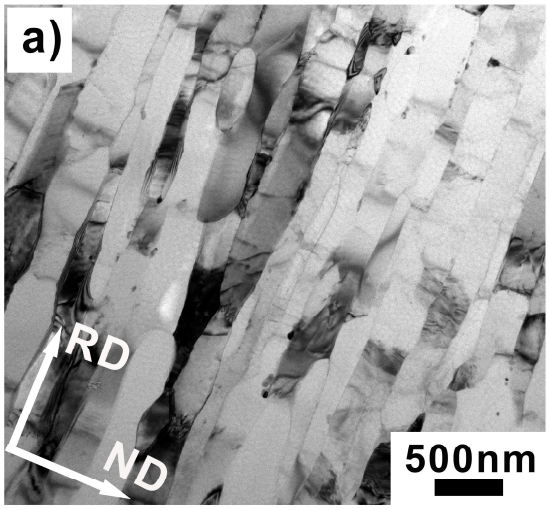

Microstructure of Al-0.3%Cu cold rolled to 98%

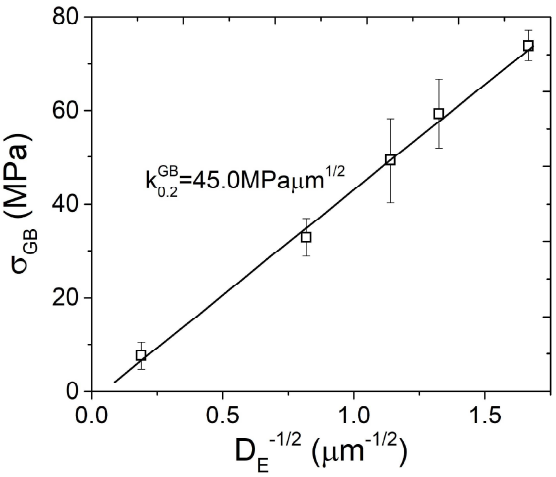

H-P relationship between contribution of boundary strengthening and equivalent boundary spacing

Table 1

Treatment	D^{GNB} (μm	$f_{<3^\circ}^{GNB}$ (%)	$\theta_{<3^\circ,av}^{GNB}$ (°)	D^{IDB} (μm)	$f_{<3^\circ}^{IDB}$ (%)	$\theta_{<3^\circ,av}^{IDB}$ (°)	$\frac{D^{IDB}}{D^{GNB}}$	D_E (μm) [a]	ρ_0 (10^{14} m^{-2})	ρ_{LB} (10^{14} m^{-2}) [b]
As deformed	0.20	3.7	1.94	0.78	67.2	1.63	3.4	0.36	1.75 ± 0.05	2.34 ± 0.12
100 □	0.32	8.2	2.13	0.98	60.0	1.73	3.1	0.57	1.44 ± 0.14	2.02 ± 0.09
150 □	0.51	1.1	2.07	1.23	45.5	1.52	2.4	0.77	1.21 ± 0.10	0.85 ± 0.01
175 □ [c]	0.65	0	0	1.37	41.5	1.80	2.1	1.49	0.65 ± 0.09	0.78 ± 0.02
250 □	-	-	-	-	-	-	-	28.0	-	-

[a] Equivalent boundary spacing

[b] Density of dislocations stored in low angle boundaries (< 3°)

[c] non-recrystallized area

Table 1. Structural parameters in the cold rolled and annealed samples

Table 2

	$\sigma_{0.2}$ (MPa)	σ_{UTS} (MPa)	$e_{uniform}$ (%)	e_{total} (%)	V_{Rex} (%)
As-deformed	198.1	224.2	2.3	4.3	0
100 □	169.3	199.9	2.5	5.0	0
150 □	139.3	155.0	3.0	5.0	0
175 □	104.8	122.8	5.6	12.8	14
250 □	25.0	69.6	27.5	28.2	100

Table 2. Mechanical properties of cold rolled and annealed samples

Table 3

Alloy	Purity (%)	Cu concentration (wt.%)	Treatment	Strain	d_t (μm) [a]	ρ_0 ($10^{14}\ m^{-2}$)	$\sigma_{0.2}$ (MPa)
Al-1%Si [36]	99	<0.0005	98% cold rolling	4.5	0.23	0.6	210
99.99%Al [11]	99.99	0.001	6 cycles ARB	4.8	0.43	0.12	96.8
AA1050 [12]	99.5	0.003	6 cycles ARB	4.8	0.40	1.0	135
AA8011 [37]	98.6	0.01	8 cycles ARB	6.4	0.32	-	200
AA1100 [9]	99.2	0.11	6 cycles ARB	4.8	0.19	1.3	234
Al-0.3%Cu	99.7	0.3	98% cold rolling	4.5	0.20	1.75	198
Al-2.5%Cu [23]	97.5	2.5	12 cycles ARB+150 □ aged	9.6	0.46	8.1	365

[a] Boundary spacing measured along the ND for the rolled samples or random spacing for the ECAP sample

Table 3. Effect of Cu concentration on grain size and dislocation density

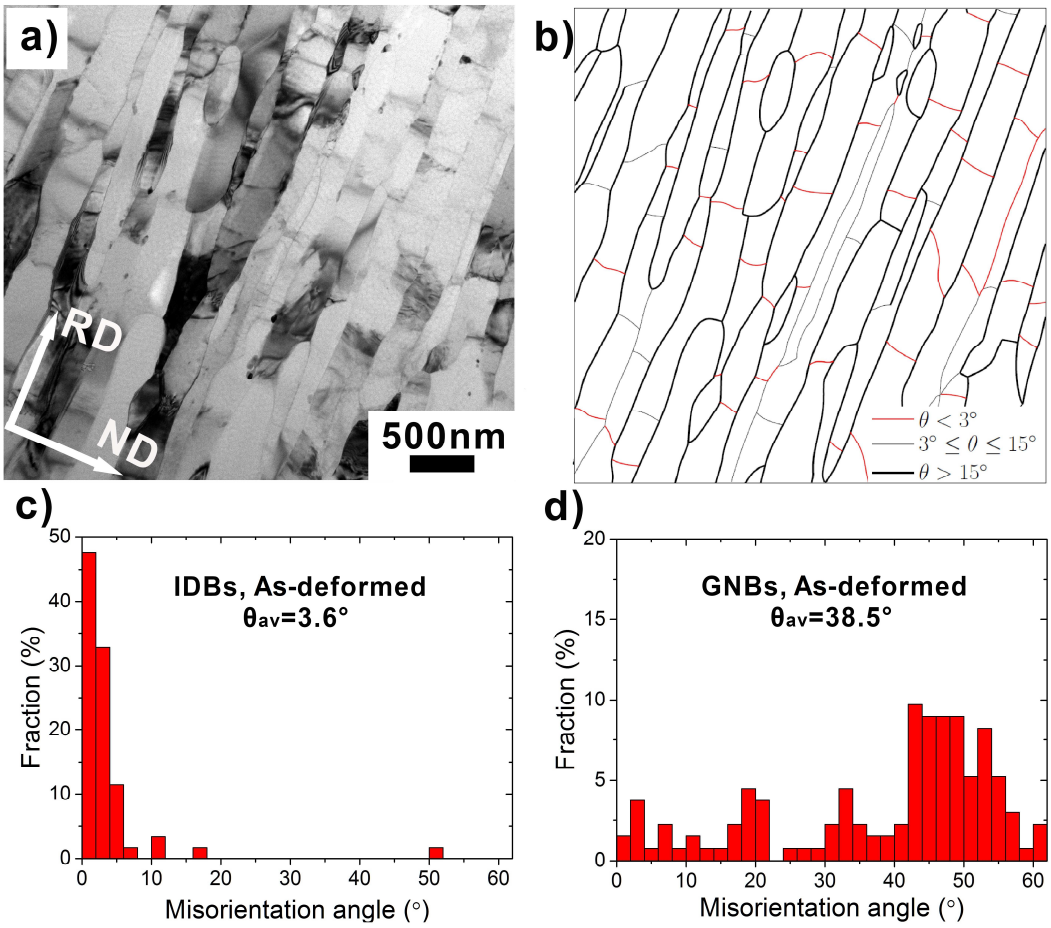

Fig. 1. Al-0.3%Cu cold rolled to 98%: a) TEM micrograph taken from the longitudinal (ND/RD) section b) Sketch showing lamellar boundaries (GNBs) and interconnecting incidental dislocation boundaries (IDBs) c) misorientation angle distribution of the IDBs and d) misorientation angle distribution of the GNBs.

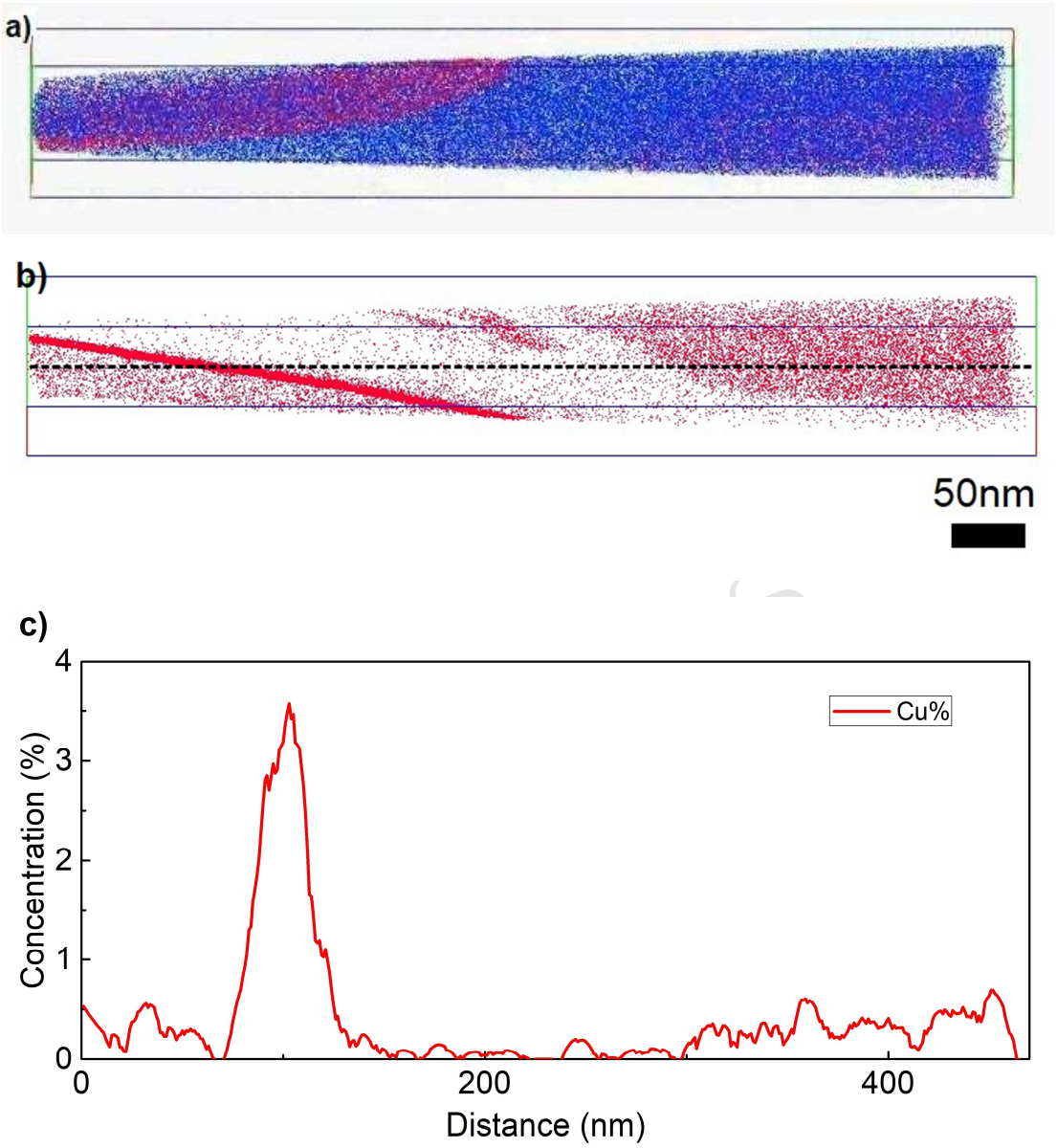

Fig. 2. 3DAP map of 98% cold rolled Al-0.3%Cu alloy: a) atom probe reconstructions with Al atoms shown in blue and Cu atoms in red b) atom probe reconstructions showing only Cu atoms as viewed from a direction with the grain boundary perpendicular to the paper surface c) Cu concentration along the dashed line indicated in b).

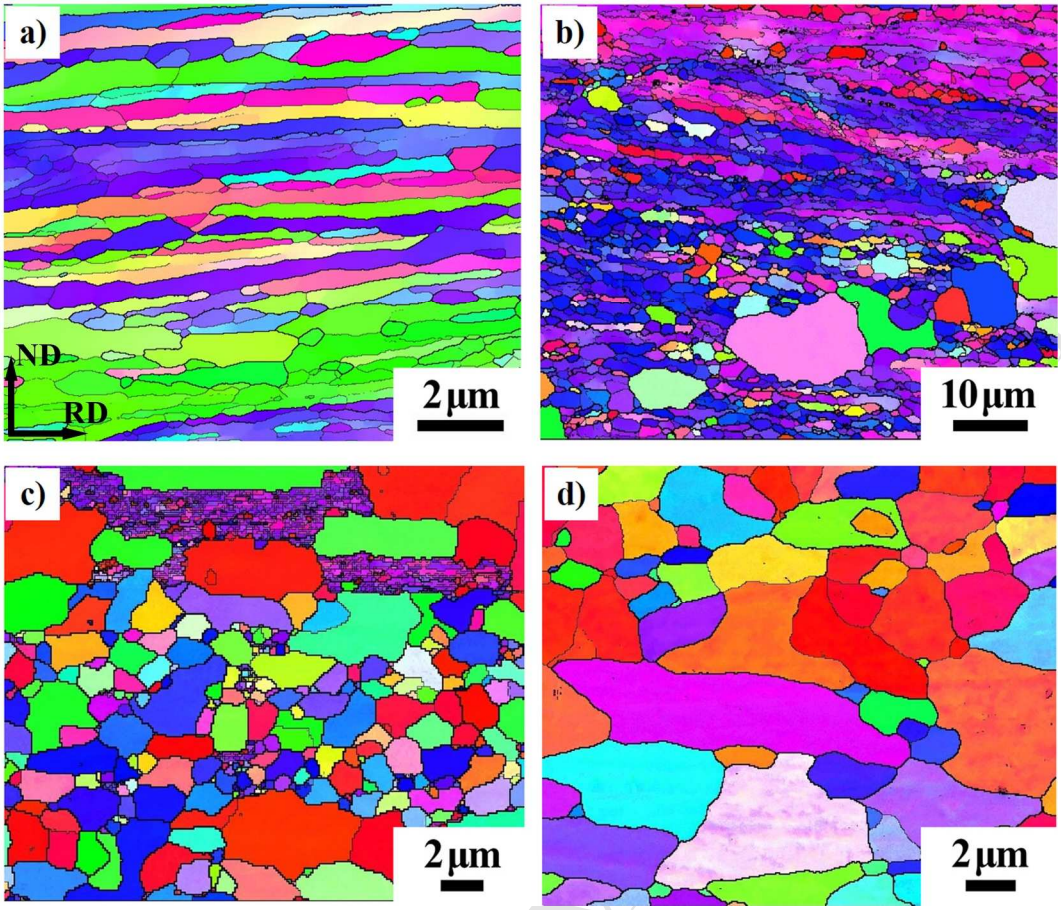

Fig. 3. EBSD maps of the samples annealed at different temperatures for 1 hour: a) 100 □ b) 175 □ c) 200 □ d) 225 □.

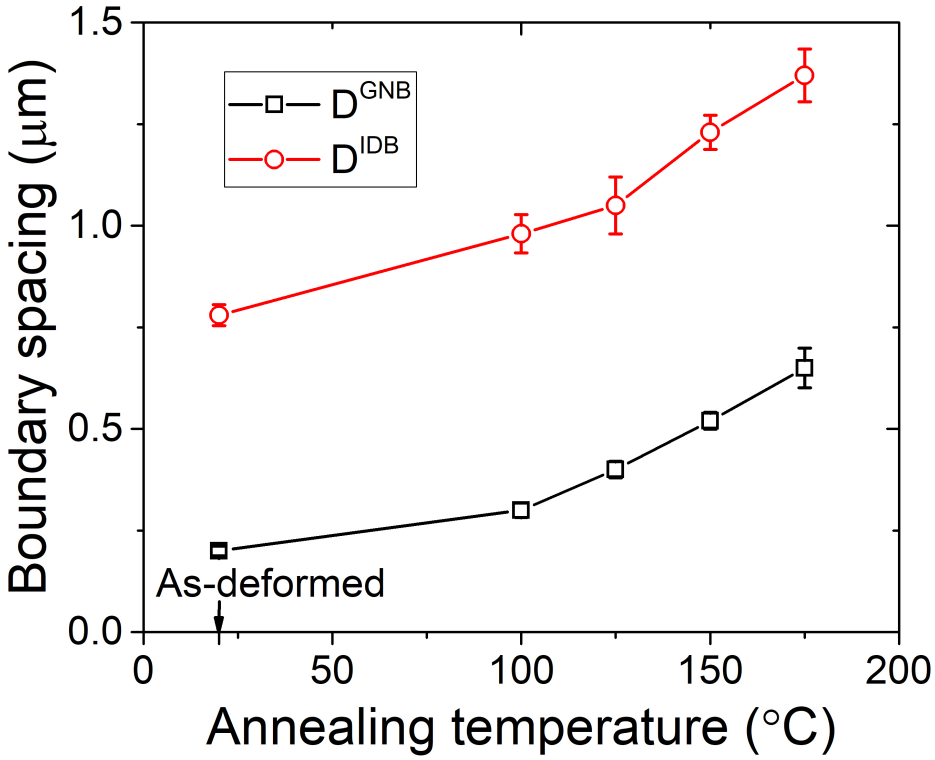

Fig. 4. Effect of annealing temperature on GNBs spacing and IDBs spacing, note that for the 175 ℃ annealed sample, only data for non-recrystallized area are given.

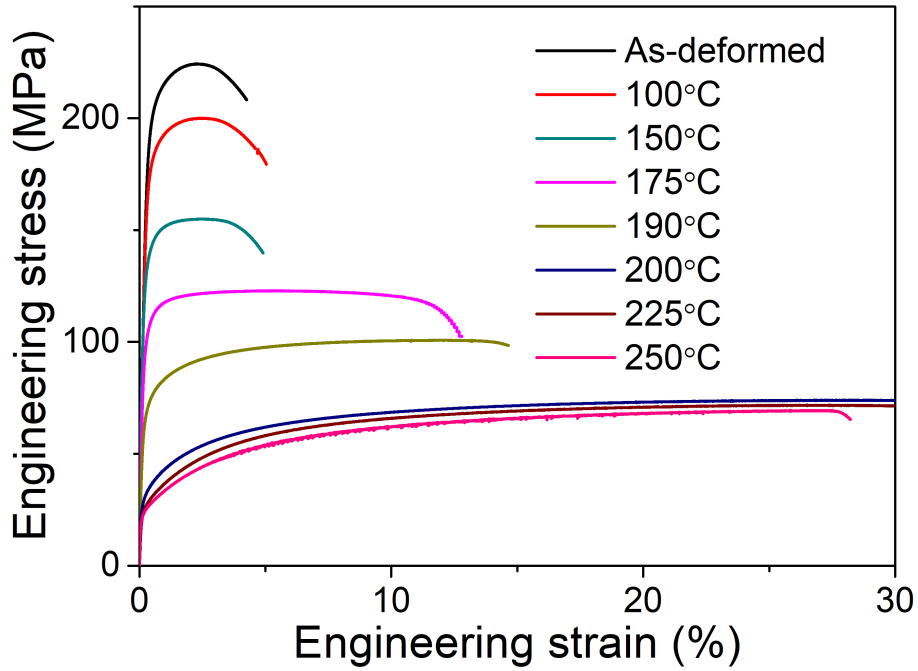

Fig. 5. Stress-strain curves of the as deformed and annealed Al-0.3%Cu alloy. [19]

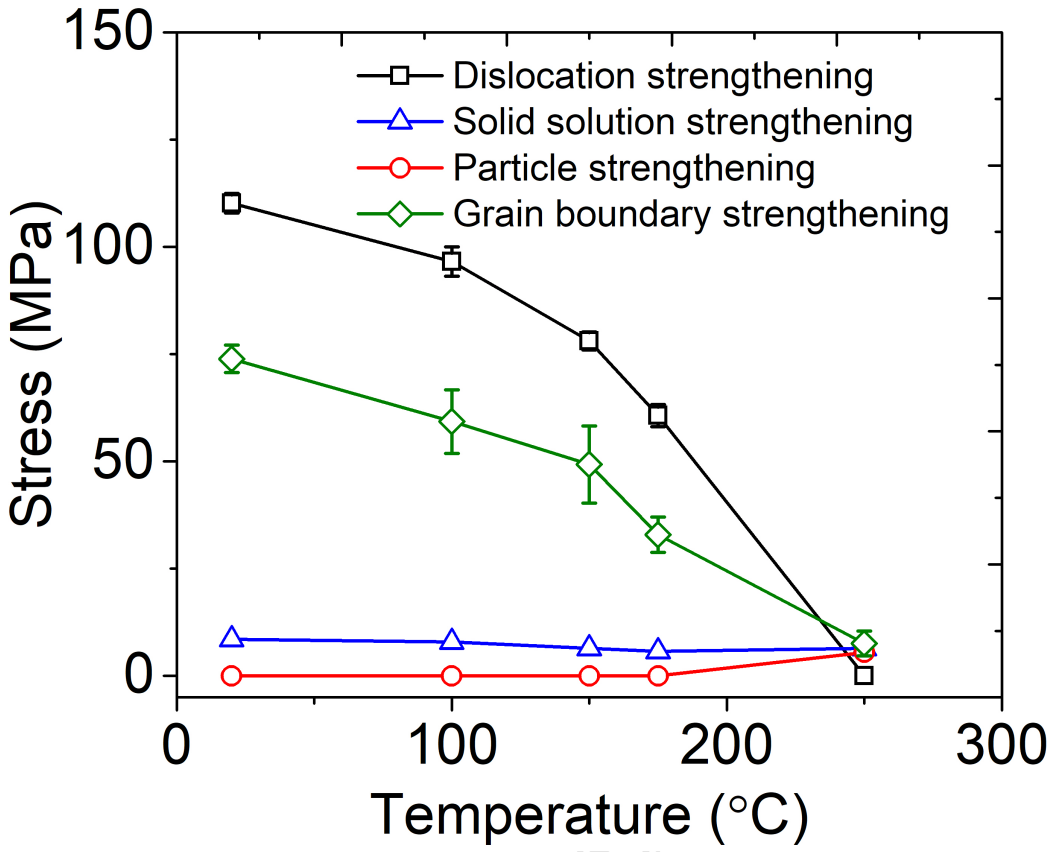

Fig. 6. Effect of annealing temperature on strengthening contributions from different mechanisms.

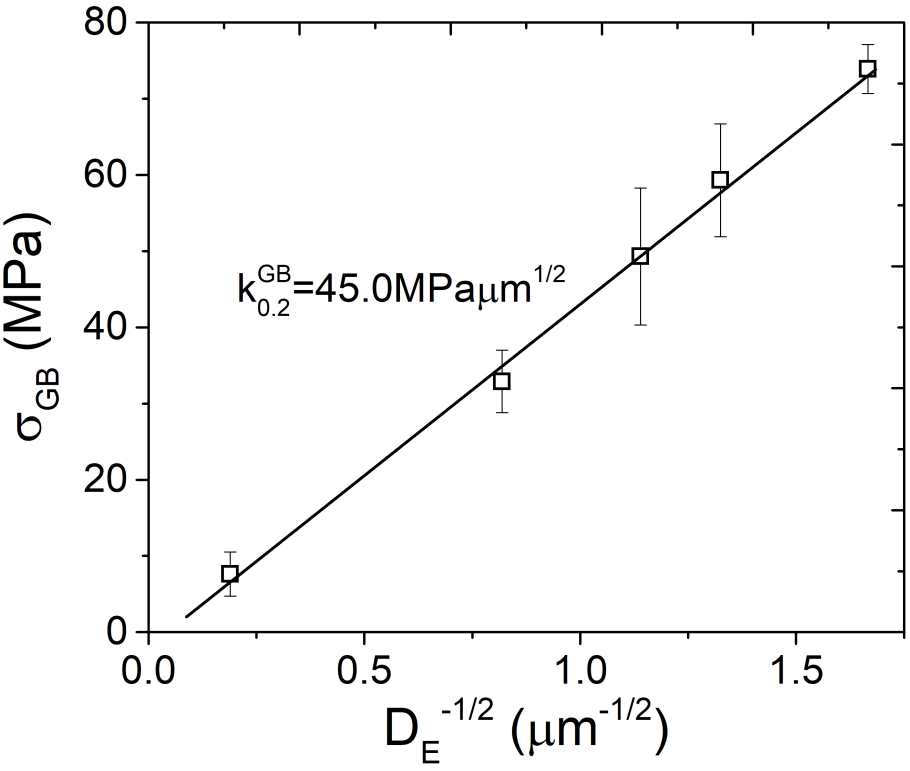

Fig. 7. The calculated grain boundary strengthening contribution to strength VS. the reciprocal square root of the equivalent boundary spacing.

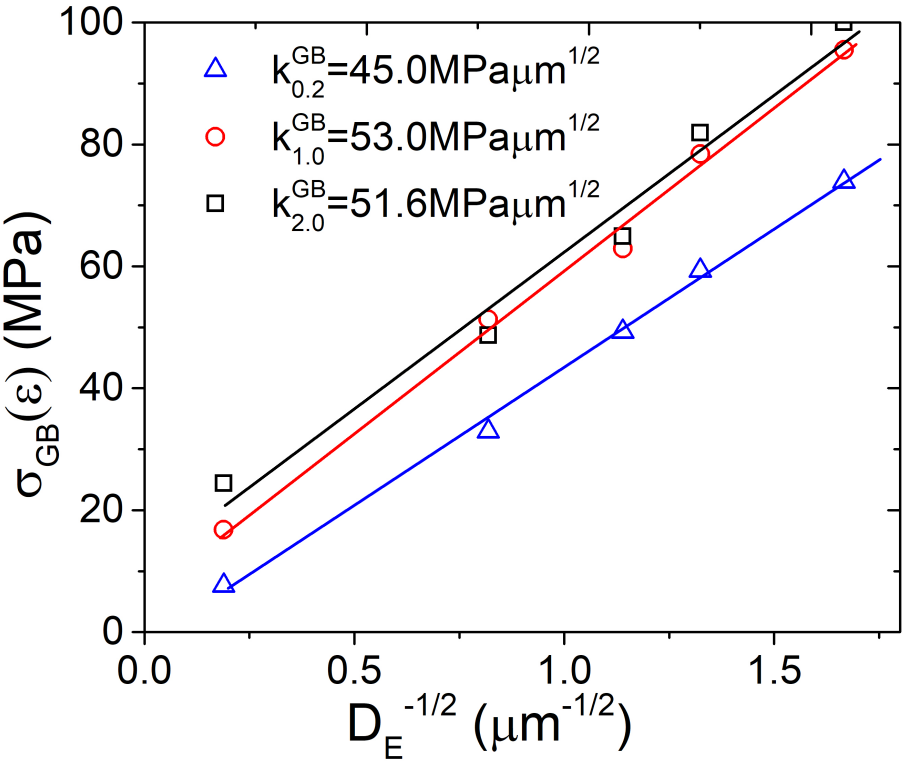

Fig. 8. Hall-Petch plot for different offset strain of Al-0.3%Cu. The Hall-Petch slopes show a slight increase with offset strain.